Relativistic convergent close-coupling calculation of inelastic scattering of electrons from cesium

Christopher J. Bostock,* Dmitry V. Fursa, and Igor Bray
ARC Centre for Antimatter-Matter Studies, Curtin University, GPO Box U1987, Perth, WA 6845, Australia
(Received 19 February 2014; published 24 March 2014)

We present fully relativistic convergent close-coupling calculations of differential cross sections, spin-asymmetries, and Stokes parameters for inelastic electron-cesium scattering at intermediate energies. Comparison is made with the differential cross section and spin asymmetry measurements of Baum *et al*. [Phys. Rev. A **70**, 012707 (2004)] and the Stokes parameter measurements of Slaughter *et al*. [Phys. Rev. A **75**, 062717 (2007)]. Comparison is also made with previous semirelativistic and nonrelativistic theories. With a relatively high atomic number for cesium ($Z = 55$) we find surprisingly excellent agreement between the relativistic, semirelativistic, and nonrelativistic theories for most observables. The overall agreement with the measurements is very good, with isolated discrepancies for some observables.

DOI: 10.1103/PhysRevA.89.032712 PACS number(s): 34.80.Dp, 34.80.Nz

I. INTRODUCTION

The extensive set of inelastic electron-Cs spin asymmetry measurements by Baum *et al*. [1] were performed to serve as a benchmark for scattering theories. Hitherto, only the semirelativistic R-matrix and nonrelativistic convergent close-coupling methods described in Ref. [1] have been applied to *inelastic* electron-Cs scattering for comparison with the measurements. With a significantly high atomic number ($Z = 55$) for Cs, there is motivation for a fully relativistic approach. Of particular interest are the results for the "relativistic" spin asymmetries A_1 and A_2 which, according to the analysis of Andersen and Bartschat [2], are identically zero in a nonrelativistic calculation. A_1 is obtained for unpolarized electrons scattered from a spin-polarized target, and A_2 is obtained for polarized electrons scattered from unpolarized targets. The exchange asymmetry A_{nn} on the other hand is nonzero in nonrelativistic calculations. This measures the relative difference between differential cross sections for parallel and antiparallel orientation of projectile and target spin polarizations. In addition to spin asymmetries, the measurement of Stokes parameters also provide a sensitive test of scattering theories because they provide information on both the magnitude and phase of scattering amplitudes [3,4].

The relativistic convergent close-coupling (RCCC) method has been applied to both elastic and inelastic electron scattering from a range of heavy quasi one- and two-electron atomic targets [5–9] and is particularly suited to calculating spin-related observables such as spin asymmetries and Stokes parameters. The method is based on employing the Dirac equation for both the target and projectile and therefore spin is accounted for in an entirely *ab initio* manner. Furthermore, the unitarity of the close coupling formalism ensures that coupling between elastic and inelastic channels is accurately accounted for within the formalism.

The RCCC method has already been applied to *elastic* e-Cs scattering [10,11]. The same model is applied here to calculate inelastic $(6s)\ ^2S_{1/2} \rightarrow (6p)\ ^2P_{1/2}$ and $(6s)\ ^2S_{1/2} \rightarrow (6p)\ ^2P_{3/2}$ scattering observables.

II. METHOD

Comprehensive details of the RCCC method for both quasi one- and two-electron targets are given in Ref. [12] and the details of the method for electron scattering on a Cs target are described in Ref. [11]. Briefly, the cesium atom is modeled as one active valence electron above an inert Xe Dirac-Fock core. The Xe Dirac–Fock core orbitals are obtained using the GRASP package [13]. For the valence electron, a set of one-electron orbitals is obtained by diagonalization of the Cs quasi one-electron Dirac–Coulomb Hamiltonian in a relativistic (Sturmian) L-spinor basis [14] with an exponential falloff $\lambda = 3.0$. A phenomenological one-electron polarization potential was used to improve the accuracy of the calculated cesium wave functions [15,16]; this allows us to take into account more accurately the effect of closed inert shells on the active electron. The polarized-orbital method of McEachran *et al*. [17] was used to produce the polarization potential from the core orbitals. Our Cs target model consists of 75 states for the active electron: $6s$–$16s$, $6p_j$–$16p_j$, $5d_j$–$15d_j$, and $4f_j$–$13f_j$ $(j = l \pm 1/2)$, comprising 27 bound states and 48 continuum states. The energy levels of the first 10 states used in the calculations are listed in Table I, and the oscillator strengths for the $(6s)\ ^2S_{1/2} \rightarrow (6p)\ ^2P_{1/2}$ and $(6s)\ ^2S_{1/2} \rightarrow (6p)\ ^2P_{3/2}$ resonance transitions are listed in Table II. Our target structure is sufficiently accurate for the purpose of facilitating a scattering calculation that includes a large number of continuum states. More accurate target-structure calculations are available for Cs [18]; however, these do not model the continuum sufficiently accurately for a comprehensive calculation of electron scattering. The capacity of the RCCC method to model the continuum accurately for a large scale scattering calculation is offset by a reduction in the accuracy of the target structure.

For the scattering calculation, the generated target states are used to expand the total wave function of the electron-Cs scattering system and formulate a set of relativistic Lippmann–Schwinger equations for the T-matrix elements. In this latter

*c.bostock@curtin.edu.au

step, the relativistic Lippmann–Schwinger equations for the T-matrix elements have the following partial wave form:

$$T_{fi}^{\Pi J}(k_f\kappa_f,k_i\kappa_i) = V_{fi}^{\Pi J}(k_f\kappa_f,k_i\kappa_i) + \sum_n \sum_\kappa \int\!\!\!\!\!\!\diagup dk \frac{V_{fn}^{\Pi J}(k_f\kappa_f,k\kappa) T_{ni}^{\Pi J}(k\kappa,k_i\kappa_i)}{E - \epsilon_n^N - \epsilon_{k'} + i0}. \tag{1}$$

The notation in Eq. (1), the matrix elements, and the method of solution using a hybrid OpenMP-MPI parallelization suitable for high performance supercomputing architectures are given in Ref. [12]. The T-matrix elements obtained from solution of Eq. (1) are used to determine the scattering amplitudes

$$F_{m_f m_i}^{\mu_f \mu_i}(\theta) = -\sum_{\kappa_f \kappa_i J \Pi} i^{L_i - L_f} e^{i\eta_{\kappa_f} + i\eta_{\kappa_i}} C_{L_f M_f, \frac{1}{2}\mu_f}^{j m_j} C_{L_i 0, \frac{1}{2}\mu_i}^{j' \mu_i} C_{j m_j, j_f m_f}^{J M_J} C_{j' \mu_i, j_i m_i}^{J M_J}$$

$$\times Y_{L_f}^{M_f}(\hat{\boldsymbol{k}}_f) \sqrt{\frac{2L_i+1}{4\pi}} T_{fi}^{\Pi J}(k_f\kappa_f,k_i\kappa_i) \sqrt{\frac{k_f}{k_i}} \sqrt{\frac{E_f E_i}{c^4}} (2\pi)^2, \tag{2}$$

where $m_j = m_i + \mu_i - m_f$ and $M_f = m_j - \mu_f$. The phase $\eta_\kappa = \sigma_\kappa + \delta_\kappa$ consists of the Dirac–Coulomb phase shift σ_κ and the distorted-wave phase shift δ_κ. The Dirac–Coulomb phase σ_κ is zero for the case of scattering from a neutral target such as Cs.

The scattering amplitudes in turn are used to calculate observables of interest. The spin-asymmetry parameters A_i can be expressed in terms of differential cross sections in the following way [20]:

$$A_1 = \left[q\left(\frac{1}{2},\frac{1}{2}\right) + q\left(\frac{1}{2},-\frac{1}{2}\right) - q\left(-\frac{1}{2},\frac{1}{2}\right) - q\left(-\frac{1}{2},-\frac{1}{2}\right) \right] \Big/ 4q_u, \tag{3}$$

$$A_2 = \left[q\left(\frac{1}{2},\frac{1}{2}\right) + q\left(-\frac{1}{2},\frac{1}{2}\right) - q\left(\frac{1}{2},-\frac{1}{2}\right) - q\left(-\frac{1}{2},-\frac{1}{2}\right) \right] \Big/ 4q_u, \tag{4}$$

$$A_{nn} = \left[q\left(\frac{1}{2},-\frac{1}{2}\right) + q\left(-\frac{1}{2},\frac{1}{2}\right) - q\left(\frac{1}{2},\frac{1}{2}\right) - q\left(-\frac{1}{2},-\frac{1}{2}\right) \right] \Big/ 4q_u, \tag{5}$$

where the magnetic sublevel differential cross section is defined as

$$q(m_i\mu_i) = (2\pi)^4 \frac{k_f}{k_i} \frac{\epsilon_f \epsilon_i}{c^4} \sum_{\mu_f m_f} \left| F_{m_f m_i}^{\mu_f \mu_i}(\theta) \right|^2, \tag{6}$$

with

$$q_u(\theta) = \frac{d\sigma}{d\Omega} = \frac{1}{4}\left[q\left(\frac{1}{2},-\frac{1}{2}\right) + q\left(-\frac{1}{2},\frac{1}{2}\right) + q\left(\frac{1}{2},\frac{1}{2}\right) + q\left(-\frac{1}{2},-\frac{1}{2}\right) \right]. \tag{7}$$

The calculation of the Stokes parameters P_1, P_2, P_3, and P^+ from the scattering amplitudes is done with the aid of the density matrix formalism [21,22]. The appendix in Ref. [6] contains an explicit derivation.

The spin asymmetries A_1 and A_2 for optically allowed transitions can exhibit anomalous oscillatory behavior if insufficient partial waves are used in the calculation. Therefore 30 partial waves were run at each energy and then extrapolation to 180 partial waves was performed with a geometric progression method applied to the T-matrix elements.

TABLE I. Energy levels of the first 10 Cs states calculated by diagonalizing the target in the RCCC method. Experiment levels listed by NIST [19] are also shown.

Configuration	RCCC (eV)	Experiment (eV)
$(6s)\ ^2S_{1/2}$	0.000	0.000
$(6p)\ ^2P_{1/2}$	1.384	1.386
$(6p)\ ^2P_{3/2}$	1.449	1.455
$(5d)\ ^2D_{3/2}$	1.628	1.798
$(5d)\ ^2D_{5/2}$	1.633	1.810
$(7s)\ ^2S_{1/2}$	2.299	2.298
$(7p)\ ^2P_{1/2}$	2.679	2.699
$(7p)\ ^2P_{3/2}$	2.719	2.721
$(6d)\ ^2D_{3/2}$	2.758	2.800
$(6d)\ ^2D_{5/2}$	2.761	2.805
Ionization limit	3.893	3.894

III. RESULTS

The experiment of Baum *et al.* [1] covered a considerable range of electron-Cs impact energies between 5 and 25 eV. The measurements were carried out with two different settings for the energy resolution of the scattered electrons; namely, $\Delta E_{\mathrm{FWHM}} = 0.3$ eV for resolving the $6p$- from the $5d$-state excitation and with $\Delta E_{\mathrm{FWHM}} = 0.7$ eV for giving a combined signal of the unresolved $6p$ and $5d$ excitation. The electron-impact energies at 7, 8, 9, 10, and 12 eV could resolve the

TABLE II. Oscillator strengths of the Cs ground state compared to experimental values listed by NIST [19].

Transition	Oscillator strength RCCC	Expt.
$(6s)\ ^2S_{1/2} \rightarrow (6p)\ ^2P_{1/2}$	0.398	0.344
$(6s)\ ^2S_{1/2} \rightarrow (6p)\ ^2P_{3/2}$	0.819	0.714

$6p$- from the $5d$-state excitation and therefore we present spin symmetries for the $6p$- and $5d$-state excitations at these energies. The detector could not resolve the individual $6p_{1/2}$,$6p_{3/2}$ fine structure levels nor the individual $5d_{3/2}$,$5d_{5/2}$ fine structure levels. Therefore it is necessary to take a combination of the cross sections and spin asymmetries as follows:

$$q_u^p = q_u^{p_{1/2}} + q_u^{p_{3/2}}, \tag{8}$$

$$A_i^p = \frac{q_u^{p_{1/2}} A_i^{p_{1/2}} + q_u^{p_{3/2}} A_i^{p_{3/2}}}{q_u^{p_{1/2}} + q_u^{p_{3/2}} a}, \tag{9}$$

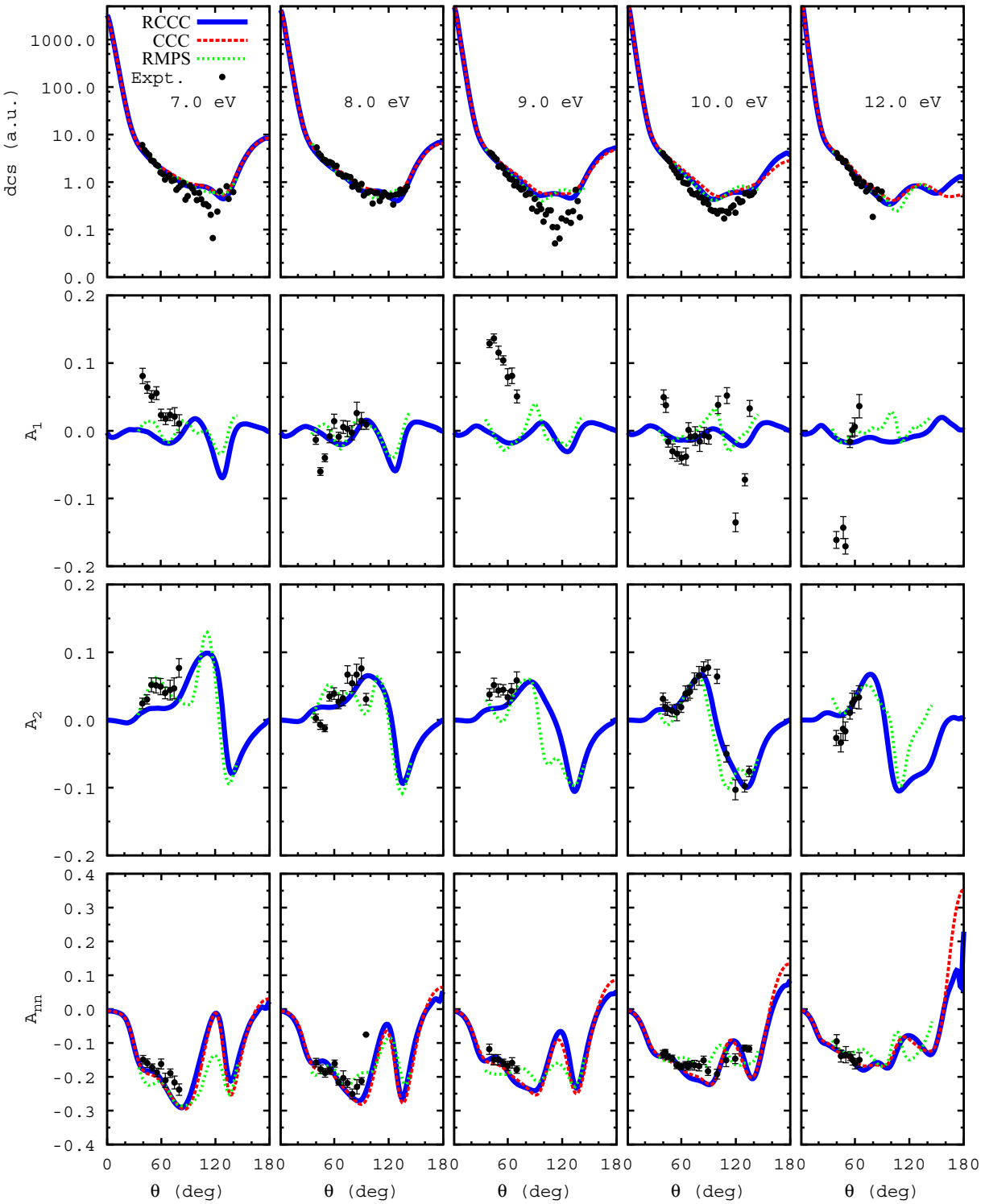

FIG. 1. (Color online) $(6s)\ ^2S_{1/2} \rightarrow (6p)\ ^2P_{1/2,3/2}$. Measurements are due to Baum *et al.* [1]. Other theories shown are a semirelativistic Breit–Pauli R-matrix method and the nonrelativistic convergent close-coupling method, also described in Ref. [1]. The differential cross sections are given in atomic units (a.u.) and the spin asymmetries are dimensionless.

and

$$q_u^d = q_u^{d_{1/2}} + q_u^{d_{3/2}}, \tag{10}$$

$$A_i^d = \frac{q_u^{d_{1/2}} A_i^{d_{1/2}} + q_u^{d_{3/2}} A_i^{d_{3/2}}}{q_u^{d_{1/2}} + q_u^{d_{3/2}}}. \tag{11}$$

Figure 1 illustrates the the electron-impact excitation $(6s)\ ^2S_{1/2} \rightarrow (6p)\ ^2P_{1/2,3/2}$ differential cross sections and spin asymmetries obtained with Eqs. (8) and (9), respectively, for electron energies 7, 8, 9, 10, and 12 eV. Comparison is made with a semirelativistic R matrix with pseudostates method (RMPS) and the nonrelativistic convergent

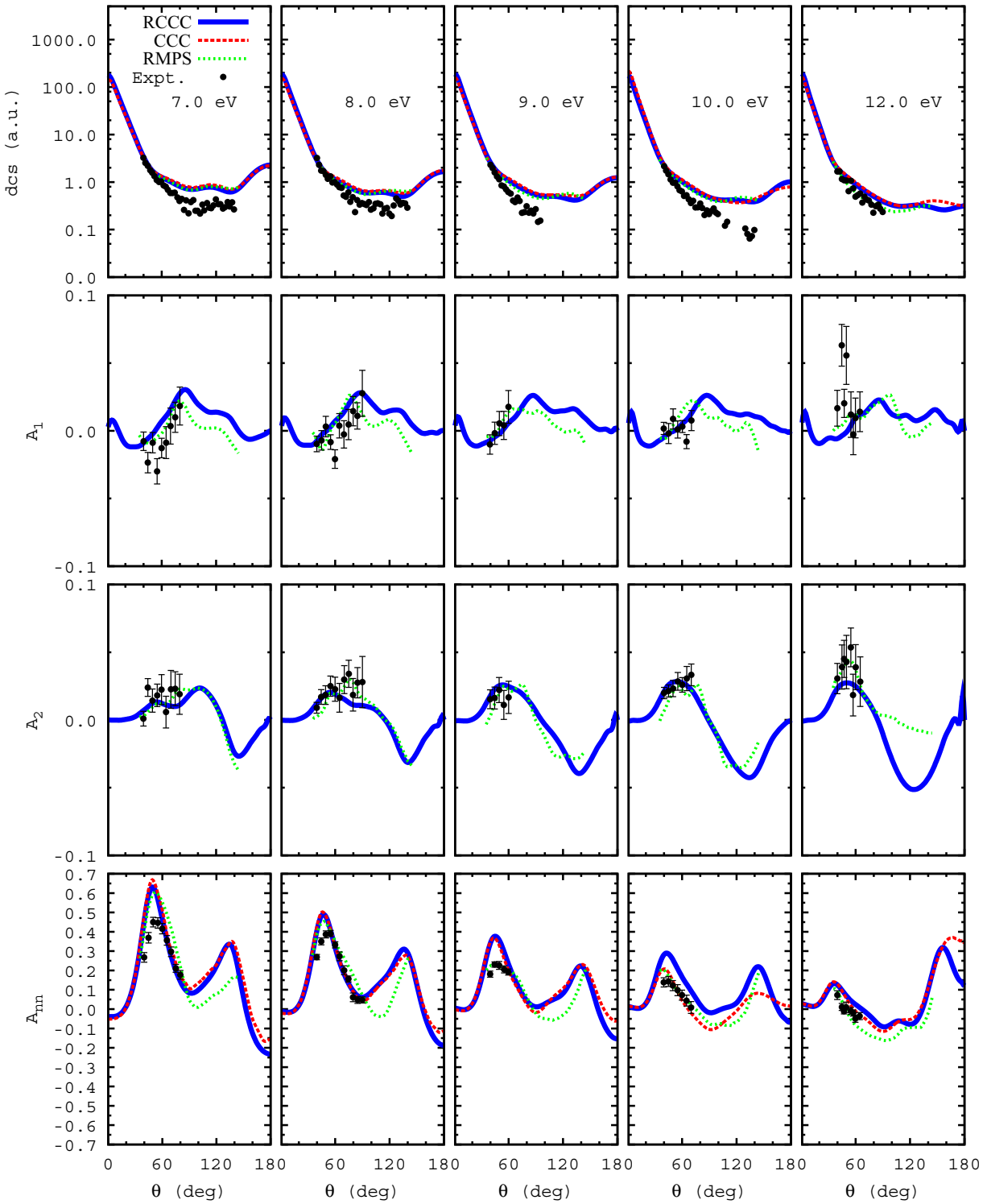

FIG. 2. (Color online) $(6s)\ ^2S_{1/2} \rightarrow (5d)\ ^2D_{3/2,5/2}$. Measurements are due to Baum *et al.* [1]. Other theories shown are a semirelativistic Breit–Pauli R-matrix method and the nonrelativistic convergent close-coupling method, also described in Ref. [1]. The differential cross sections are given in atomic units (a.u.) and the spin asymmetries are dimensionless.

close-coupling (CCC) method [1], together with the measurements of Baum *et al*. [1]. Figure 2 illustrates the corresponding information for the $(6s)\ ^2S_{1/2} \rightarrow (5d)\ ^2D_{3/2,5/2}$ transitions, employing Eqs. (10) and (11).

In general there is good agreement between the RCCC and RMPS theories across all observables in both figures. The nonrelativistic CCC method gives identically zero for A_1 and A_2 and therefore the CCC results are not shown for

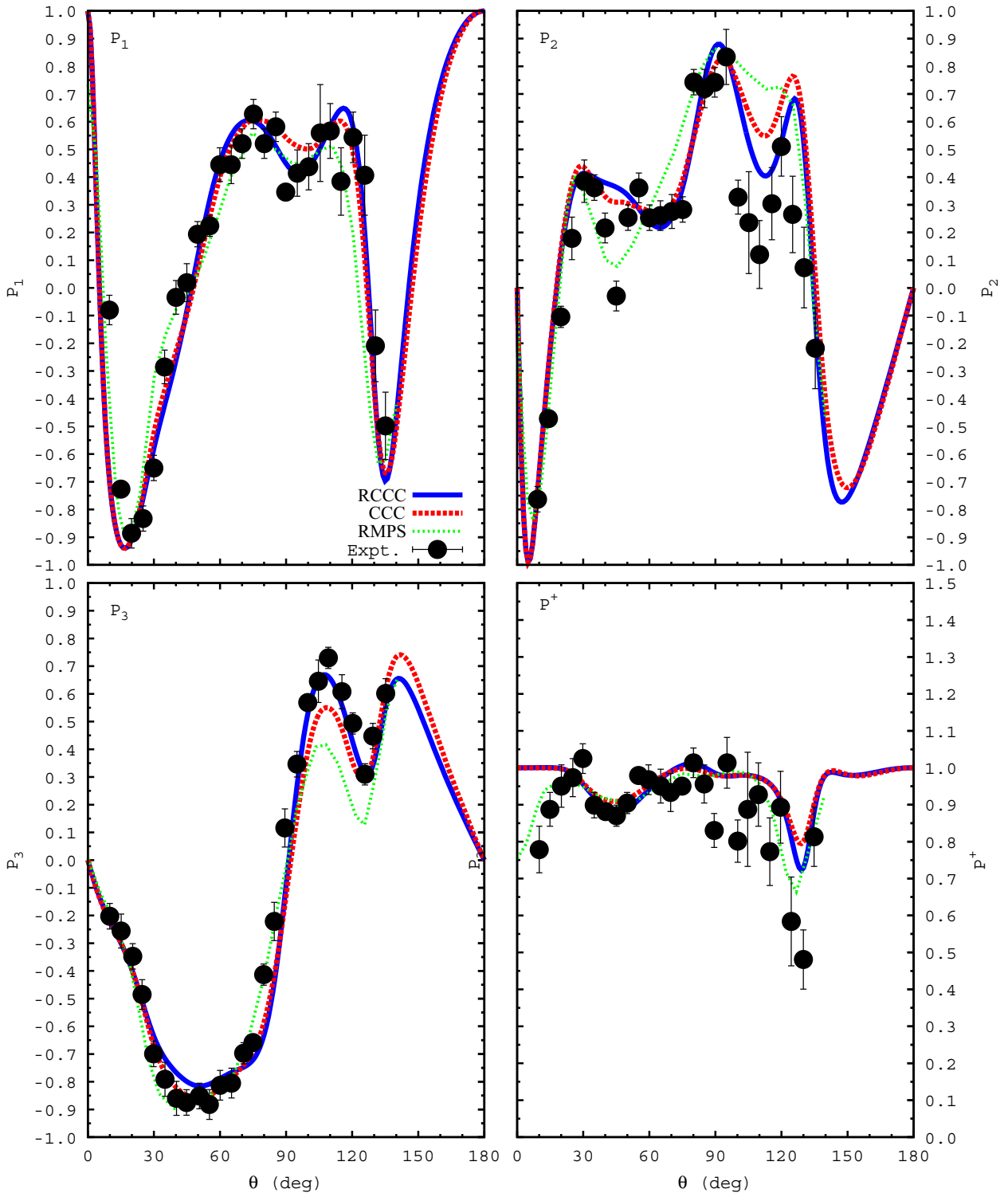

FIG. 3. (Color online) 7 eV Stokes $(6s)\ ^2S_{1/2} \rightarrow (6p)\ ^2P_{3/2}$. Measurements are due to Slaughter *et al*. [23]. Note that the measurements pertain to superelastic scattering on the $(6p)\ ^2P_{3/2}$ state where the incident energy of 5.5 eV is equivalent to 7.0 eV for the corresponding inelastic $(6s)\ ^2S_{1/2} \rightarrow (6p)\ ^2P_{3/2}$ transition. Other theories shown are a semirelativistic Breit–Pauli R-matrix method and the nonrelativistic convergent close-coupling method, also described in Ref. [23]. The Stokes parameters are dimensionless.

these observables. For the nonzero CCC observables, there is excellent agreement with the RCCC theory. In Figs. 1 and 2 the RCCC and CCC results for the differential cross section and A_{nn} are very close to each other and the lines in the figures are practically on top of each other across a wide range of angles for these observables.

While the theories are consistent with each other, the agreement between the theories and the measurements is

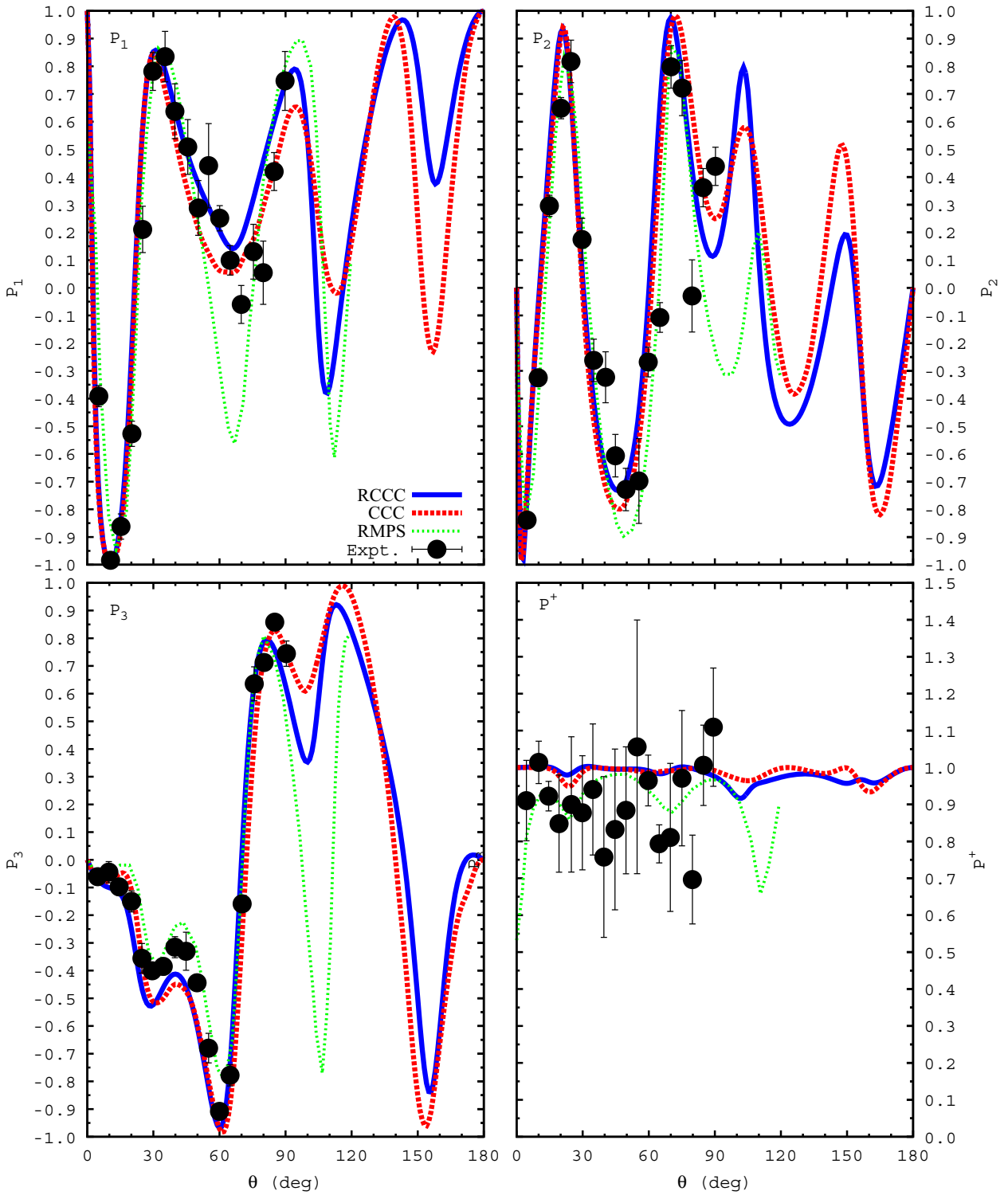

FIG. 4. (Color online) 15 eV Stokes $(6s)\ ^2S_{1/2} \rightarrow (6p)\ ^2P_{3/2}$. Measurements are due to Slaugher *et al.* [23]. Note that the measurements pertain to superelastic scattering on the $(6p)\ ^2P_{3/2}$ state where the incident energy of 13.5 eV is equivalent to 15.0 eV for the corresponding inelastic $(6s)\ ^2S_{1/2} \rightarrow (6p)\ ^2P_{3/2}$ transition. Other theories shown are a semirelativistic Breit–Pauli R-matrix method and the nonrelativistic convergent close-coupling method, also described in Ref. [23]. The Stokes parameters are dimensionless.

varied. Along the bottom two rows in each figure, the agreement between theory and experiment for A_{nn} and A_2 is in general very good. For the spin asymmetry A_1, on the other hand, the agreement only holds in Fig. 2 at 7, 8, 9, and 10 eV. Similarly for the differential cross sections: while the theories are in agreement with each other, there are discrepancies between theory and experiment in Fig. 1 at 7, 9, and 10 eV, and in Fig. 2 at 7, 8, 9, and 10 eV. Given the agreement between rather diverse theories, and the internal checking of convergence, we are unable to explain the origin of the identified discrepancies. An independent experiment to repeat the measurements could provide a further consistency check.

In Figs. 3 and 4 we present Stokes parameters at 7 and 15 eV, respectively, for comparison with the superelastic measurements of Slaughter *et al*. [23] for the $(6s)\ ^2S_{1/2} \rightarrow (6p)\ ^2P_{3/2}$ transition. The RCCC fine-structure-resolved results for P_1 and P_2 had to be divided by 0.6 [24] in order to be able to compare with the presented results in Slaughter *et al*. [23] for an $S \rightarrow P$ transition. The 7 eV Stokes parameters illustrated in Fig. 3 indicate that there is excellent agreement between the three theories and also with the measurements. In Fig. 4 there is excellent agreement between the RCCC and CCC results and the measurements. The RMPS results are in also in agreement, except some of the RMPS minima are too deep.

IV. CONCLUSION

We have presented a range of RCCC results in order to provide comparison with the inelastic electron-Cs scattering experiments of Baum *et al*. [1] and Slaughter *et al*. [23]. We also compared the fully relativistic RCCC results with the previous semirelativistic RMPS and nonrelativistic CCC calculations. In general, there is excellent agreement among the three theories. Agreement between the RCCC results and the measurements is excellent for the Stokes parameters, and spin asymmetries A_{nn} and A_2. For the spin asymmetry A_1, and the differential cross sections, some discrepancies exist at certain energies between the RCCC results and the measurements. It is interesting to highlight that Cs, with $Z = 55$, is modeled very well with the nonrelativistic CCC method for inelastic electron scattering differential cross sections, A_{nn} and Stokes parameters; only spin asymmetries A_1 and A_2 are identically zero in the nonrelativistic formalism.

ACKNOWLEDGMENTS

Support of the Australian Research Council and Curtin University is acknowledged. We are grateful for access to the Australian National Computational Infrastructure and its Western Australian node iVEC.

[1] G. Baum, S. Förster, N. Pavlović, B. Roth, K. Bartschat, and I. Bray, Phys. Rev. A **70**, 012707 (2004).
[2] N. Andersen and K. Bartschat, J. Phys. B **35**, 4507 (2002).
[3] B. Bederson, Comments At. Mol. Phys. **1**, 41 (1969).
[4] B. Bederson, Comments At. Mol. Phys. **1**, 65 (1969).
[5] C. J. Bostock, M. J. Berrington, D. V. Fursa, and I. Bray, Phys. Rev. Lett. **107**, 093202 (2011).
[6] C. J. Bostock, D. V. Fursa, and I. Bray, Phys. Rev. A **88**, 062707 (2013).
[7] C. J. Bostock, D. V. Fursa, and I. Bray, J. Phys. B **45**, 181001 (2012).
[8] C. J. Bostock, D. V. Fursa, and I. Bray, Phys. Rev. A **85**, 062707 (2012).
[9] C. J. Bostock, D. V. Fursa, and I. Bray, Phys. Rev. A **86**, 062701 (2012).
[10] D. V. Fursa and I. Bray, Phys. Rev. Lett. **100**, 113201 (2008).
[11] D. V. Fursa, C. J. Bostock, and I. Bray, Phys. Rev. A **80**, 022717 (2009).
[12] C. J. Bostock, J. Phys. B **44**, 083001 (2011).
[13] K. G. Dyall, I. P. Grant, C. T. Johnson, F. P. Parpia, and E. P. Plummer, Comp. Phys. Comm. **55**, 425 (1989).
[14] I. P. Grant and H. M. Quiney, Phys. Rev. A **62**, 022508 (2000).
[15] D. V. Fursa and I. Bray, J. Phys. B **30**, 5895 (1997).
[16] D. V. Fursa, I. Bray, and G. Lister, J. Phys. B **36**, 4255 (2003).
[17] R. P. McEachran, D. L. Morgan, A. G. Ryman, and A. D. Stauffer, J. Phys. B **10**, 663 (1977).
[18] A. Sieradzan, M. D. Havey, and M. S. Safronova, Phys. Rev. A **69**, 022502 (2004).
[19] http://physics.nist.gov/PhysRefData/ASD/levels_form.html.
[20] K. Bartschat and Y. Fang, Phys. Rev. A **62**, 052719 (2000).
[21] V. Balashov, A. Grum-Grzhimailo, and N. Kabachnik, *Polarization and Correlation Phenomena in Atomic Collisions: A Practical Theory Course*, Physics of Atoms and Molecules (Springer, New York, 2000).
[22] K. Blum, *Density Matrix Theory and Applications* (Plenum Press, New York, 1981).
[23] D. S. Slaughter, V. Karaganov, M. J. Brunger, P. J. O. Teubner, I. Bray, and K. Bartschat, Phys. Rev. A **75**, 062717 (2007).
[24] N. Andersen, J. W. Gallagher, and I. V. Hertel, Phys. Rep. **165**, 1 (1988).